Multimed Tools Appl (2018) 77:12853–12869
DOI 10.1007/s11042-017-4919-z

Image compressed sensing based on non-convex low-rank approximation

Yan Zhang [1,2] · Jichang Guo [1] · Chongyi Li [1]

Received: 19 July 2016 / Revised: 13 April 2017 / Accepted: 5 June 2017 /
Published online: 30 June 2017

Abstract Nonlocal sparsity and structured sparsity have been evidenced to improve the reconstruction of image details in various compressed sensing (CS) studies. The nonlocal processing is achieved by grouping similar patches of the image into the groups. To exploit these nonlocal self-similarities in natural images, a non-convex low-rank approximation is proposed to regularize the CS recovery in this paper. The nuclear norm minimization, as a convex relaxation of rank function minimization, ignores the prior knowledge of the matrix singular values. This greatly restricts its capability and flexibility in dealing with many practical problems. In order to make a better approximation of the rank function, the non-convex low-rank regularization namely weighted Schatten *p*-norm minimization (WSNM) is proposed. In this way, both the local sparsity and nonlocal sparsity are integrated into a recovery framework. The experimental results show that our method outperforms the state-of-the-art CS recovery algorithms not only in PSNR index, but also in local structure preservation.

Keywords Image compressed sensing · Low-rank approximation · Weighted Schatten *p*-norm · Non-convex optimization

✉ Jichang Guo
jchguotju@163.com

Yan Zhang
zhangyantju@tju.edu.cn

Chongyi Li
lichongyi@tju.edu.cn

[1] School of Electronic Information Engineering, Tianjin University, 92 Weijin Road, Nankai District, Tianjin 300072, China

[2] School of Computer and Information Engineering, Tianjin Chengjian University, 26 Jinjing Road, Xiqing District, Tianjin 300384, China

1 Introduction

The Compressive sensing [6, 15, 24] theory states that a signal can be reconstructed from a small set of random projections, provided that it is sparse in some linear transform domain. For example, a finite discrete signal has K nonzero transform coefficients with $K << N$, where N is the dimension of the transform space. This theory has a wide range of applications in signal processing, information theory, computer science, and electrical engineering [27, 31, 42].

Conventional CS recovery exploits the l_1-norm based sparsity of a signal. Recently, many authors have shown that the solution of l_p-norm sparse coding with $0 < p < 1$ is close to that of the l_1-minimization and it is sparser, and thus l_p-minimization allows exact recovery of signals from much fewer linear measurements [17, 35]. Since enhancing the sparsity has been evidenced to improve the reconstruction of image details, the concept of sparsity has evolved into various sophisticated forms including the nonlocal sparsity [13] and structured/group sparsity [19]. The nonlocal processing is achieved by grouping similar patches of the image into the groups. Exploiting the nonlocal self-similarity has led to the well-known nonlocal means methods [2], block-matching 3D denoising (BM3D) [10] and simultaneous sparse coding (SSC) [26]. And nonlocal sparsity has been widely used in the areas of image restoration. [20, 25, 36]. Since the group is formed with a set of similar image patches, the rank of this group is low. Therefore, in this paper, the low-rank approximation is utilized to characterize the nonlocal sparsity of natural images. In [14], the nonlocal low-rank regularization was proposed for CS, called as NLR-CS. And the log det$(\boldsymbol{X})$ was used to solve the problem of rank minimization.

In recent years, there is a flurry of research on low-rank matrix approximation, and many important models have been proposed [8, 18, 22, 40, 41]. The nuclear norm as a convex surrogate for the non-convex rank function has been attracting great research interest. However, the nuclear norm minimization (NNM) still has some problems in practice [18, 41]. The basic rank function in which all nonzero singular values have equal contributions, however, the NNM treats each singular value by adding them together. This suppresses the low-rank components and shrinks the recovered data. The truncated nuclear norm regularization (TNNR) has been introduced for low-rank matrix approximation, only minimizing the smallest singular values [41]. The TNNR is not flexible enough since it makes a decision that whether to regularize a singular value or not. To improve the flexibility of the truncated nuclear norm, the weighted nuclear norm minimization (WNNM) is proposed to provide the weights to penalize the difference between matrix singular values [18]. These methods take advantage of such prior knowledge of the matrix singular values. However, they are not convex in general case, and it is more difficult to solve than NNM. Moreover, recent advances have shown that better low-rank matrix recovery performance can be obtained by replacing nuclear norm with Schatten p-norm [23, 30, 39]. In order to make a better approximation of the rank function, this paper considers a non-convex low-rank approximation via weighted Schatten p-norm minimization (WSNM).

In this paper, a patch-wise nonlocal low-rank regularization based image compressive sensing method is presented. To exploit the nonlocal sparsity of natural images, patch grouping and low-rank approximation are utilized to regularize the CS recovery. Moreover, non-convex low-rank regularization namely WSNM is studied, and its optimal solution is analyzed. Different weights or weighting rules can be introduced based on the prior knowledge. Then an efficient optimization algorithm to solve this CS recovery problem is proposed. The simulation results on natural images demonstrate that the proposed method achieves lower reconstruction error and higher visual quality than conventional CS recovery methods.

The remainder of the paper is organized as follows. The methods of conventional CS recovery and low-rank approximation are reviewed in Section 2. The analysis of our proposed WSNM method and optimization algorithm is presented in Section 3. The CS recovery using the proposed method is analyzed in Section 4. Extensive experimental results are presented in Section 5. The conclusions are given in Section 6.

2 Background

2.1 Conventional CS

CS aims at accurately reconstructing signals from a small number of linear non-adaptive measurements by using an optimization programming process [6, 15]. Given an N dimensional signal x, the corresponding CS model can be expressed as follows:

$$x = \arg\min_{x} \|x\|_0, \quad s.t. \ y = \Phi x, \tag{1}$$

where $y \in C^M$ is the measurement vector, $\Phi \in C^{M \times N}$ $(M < N)$ is the measurement matrix. Assuming certain conditions on the matrix Φ, alternative strategies to find sparsest solutions have been put forward, such as orthogonal greedy algorithms [34] or basis pursuit [9]. However, l_0-norm minimization is a difficult combinatorial optimization problem, and it remains an NP-hard problem that cannot be solved in practice [29]. For this reason, the non-convex l_0-norm can be replaced with the convex l_1-norm. Then this problem becomes the following unconstrained optimization problem:

$$x = \arg\min_{x} \|y - \Phi x\|_2^2 + \lambda \|x\|_1. \tag{2}$$

The above l_1-minimization problem can be efficiently solved by various methods, such as Bayesian algorithm [37], iterative shrinkage algorithm [11] and alternative direction multiplier method (ADMM) [21]. Although conventional CS recovery is promising for reconstruction from measurement image, sometimes leads to an insufficient sparse representation for natural images, thus results in artifacts in the reconstruction. Thus, this paper is to explore a domain where the image reveals a high degree of sparsity in CS recovery and thus the image can be recovered faithfully.

As we all know, some natural signals have a structure on the coefficient vector in addition to sparsity, and some often exhibit rich nonlocal self-similarities structures. Based on the signals features, recent advances use nonlocal sparsity to model signals in CS theory [1, 2]. The clustering algorithm is involved into the framework of CS to gather the similar image patches into a group. This paper exploits the nonlocal sparsity in CS recovery via low-rank approximation.

2.2 Low-rank approximation

Candes and Recht [4, 8] prove that most low rank matrices can be perfectly recovered by solving a nuclear norm minimization (NNM) problem:

$$\hat{X} = \arg\min_{X} \frac{1}{2} \|Y - X\|_F^2 + \lambda \|X\|_*, \tag{3}$$

where Y is the given matrix, $\|X\|_*$ is the nuclear norm of a matrix X and its value is equal to the sum of matrix singular values, and λ is a positive constant. Cai et al. [3] presents that the NNM based low rank matrix approximation problem can be easily solved by a soft-thresholding operation on the singular values of observation matrix.

The truncated nuclear norm regularization (TNNR) is proposed for minimizing the smallest $N-r$ singular values, where N is the number of singular values and r is the rank of the matrix [41]. The truncated nuclear norm is defined as $\|X\|_{T,*}=\sum_{i=1}^{\min(m,n)}\sigma_i(X)-\sum_{i=1}^{r}\sigma_i(X)$, where $\sigma_i(X)$ means the i-th singular value of X.

In weighted nuclear norm minimization (WNNM) method [18], the singular values are assigned different weights. The weighted nuclear norm of a matrix X is defined as $\|X\|_{w,*}=\sum_i|w_i\sigma_i(X)|_1$, where $w_i\geq 0$ is a non-negative weight assigned to $\sigma_i(X)$.

3 Low-rank approximation via WSNM

In this section, we propose a new optimization framework to discover low rank matrix with WSNM. The weighted Schatten p-norm of a matrix X is defined as:

$$\|X\|_{ws}=\left(\sum_{i=1}^{\min\{n,m\}}w_i\sigma_i(X)^p\right)^{1/p}, \tag{4}$$

where $\sigma_i(X)$ is the i-th singular value of X, $\mathbf{w}=[w_1,\ldots,w_{\min\{n,m\}}]$ is a non-negative vector, $0<p\leq 1$. Then the low-rank approximation can be expressed as the following optimization:

$$\hat{X}=\arg\min_X\frac{1}{2}\|Y-X\|_F^2+\lambda\|X\|_{ws}^p, \tag{5}$$

where $\|\cdot\|_F$ denotes the Frobenious norm. For the non-convex relaxation brought by the weighted Schatten p-norm, the above problem will be much more difficult to optimize. **Lemma** 1 is given for analyzing the optimization of WSNM problem.

Lemma 1 For $Y\in R^{m\times n}$, $m\geq n$, and let $U\Sigma V^{\mathrm{T}}$ be the singular value decomposition (SVD) of Y, where $\Sigma=\mathrm{diag}(\sigma_1,\sigma_2,\cdots\sigma_n)$. The solution of the WSNM problem in Eq. (5) can be expressed as $X=U\Delta V^T$, where $\Delta=\mathrm{diag}(\delta_1,\delta_2,\cdots\delta_n)$is a non-negative matrix and $(\delta_1,\delta_2,...,\delta_n)$ is the solution of the following non-convex optimization problem:

$$\min_{\Delta}\sum_{i=1}^{n}\left(\frac{1}{2}(\delta_i-\sigma_i)^2+\lambda w_i\delta_i^p\right) \tag{6}$$

Proof. For $X\in R^{m\times n}$, $m\geq n$, its SVD can be expressed as $X=\overline{U}\Delta\overline{V}^T$, where $\overline{U}$and $\overline{V}$are unitary matrices, and $\Delta=\mathrm{diag}(\delta_1,\delta_2,\cdots\delta_n)$. Then we have

$$\min_X\ \frac{1}{2}\|Y-X\|_F^2+\lambda\|X\|_{ws}^p=\min_X\ \frac{1}{2}\|\Delta\|_F^2-tr\left(Y^TX\right)+\frac{1}{2}\|\Sigma\|_F^2+\lambda\|X\|_{ws}^p$$
$$=\min_X\ \left(\frac{1}{2}\|\Delta\|_F^2+\frac{1}{2}\|\Sigma\|_F^2+\lambda\sum_i w_i\delta_i^p\right)-\max tr\left(Y^TX\right).$$

Since when $\overline{U} = U$ and $\overline{V} = V$, $\max tr(Y^TX) = tr(\Sigma^T\Delta)$ [28], then we can obtain

$$\min_X \frac{1}{2}\|Y-X\|_F^2 + \lambda\|X\|_{ws}^p = \min_\Delta \frac{1}{2}\|\Delta\|_F^2 - tr\left(\Sigma^T\Delta\right) + \frac{1}{2}\|\Sigma\|_F^2$$

$$+ \lambda\sum_i w_i\delta_i^p = \min_\Delta \sum_{i=1}^n \left(\frac{1}{2}(\delta_i-\sigma_i)^2 + \lambda w_i\delta_i^p\right).$$

Therefore, the optimization problem in Eq. (5) can be transformed into Eq. (6).

Next, we introduce the generalized singular value soft-thresholding function for solving the Eq. (6). In [43], a generalized soft-thresholding (GST) function is proposed for solving the l_p-norm minimization in $\min_x \frac{1}{2}(y-x)^2 + \lambda|x|^p$:

$$T_p^{GST}(y;\lambda) = \begin{cases} 0, & if\,|y| \le \tau_p^{GST}(\lambda) \\ \mathrm{sgn}(y)S_p^{GST}(|y|;\lambda), & if\,|y| > \tau_p^{GST}(\lambda) \end{cases}$$

where $\tau_p^{GST}(\lambda) = (2\lambda(1-p))^{1/(2-p)} + \lambda p(2\lambda(1-p))^{(p-1)}/(2-p)$ and $S_p^{GST}(|y|;\lambda)$ is obtained by solving

$S_p^{GST}(|y|;\lambda) - y + \lambda p\left(S_p^{GST}(|y|;\lambda)\right)^{p-1} = 0.$

In the initial, let $S_p^{GST}(|y|;\lambda)^{(0)} = |y|$. Then $S_p^{GST}(|y|;\lambda)^{(k+1)} = |y| - \lambda p\left(S_p^{GST}(|y|;\lambda)^{(k)}\right)^{p-1}$. After few loops, $S_p^{GST}(|y|;\lambda)$ can be obtained. In our method, five loops are calculated. According to GST function, the optimal solution of the Eq. (6) is called the generalized singular value soft-thresholding:

$D_p^{GSVST}(\sigma_i) = T_p^{GST}(\sigma_i;\lambda w_i).$

According to **Lemma 1**, Eq. (5) can be transformed into Eq. (6) when $\overline{U} = U$ and $\overline{V} = V$. Firstly, for Y in Eq. (5) is the given matrix, and $U\Sigma V^T$ can be obtained by SVD of Y. Secondly, Δ is the solution of Eq. (6) which can be solved by $D_p^{GSVST}(\sigma_i)$. Therefore, based on the above derivation, we can see that the solution of the WSNM problem in Eq.(5) is

$$\hat{X} = UD_p^{GSVST}(\sigma_i)V^T. \tag{7}$$

4 Non-convex low-rank regularization for CS recovery

4.1 The determination of the regularization parameter

In this section, the local and nonlocal regularization are integrated into an iterative framework for the CS recovery. For a degraded image y, a sufficient number of nonlocal similar patches $y_{i,j}$ can be searched for each exemplar $\sqrt{n} \times \sqrt{n}$ patch y_i by the block matching method [10]. Then we obtain a data matrix $Y_i = [y_{i,1}, y_{i,2}, \cdots y_{i,m}]$ for each exemplar patch y_i. Although the formed data matrixes Y_i corrupted by some noise, these image patches still have similar structures, so the data matrix Y_i is low rank. According to the assumption, we have $Y_i = X_i + N_i$, where X_i denotes the patch matrices of original image, that is the low rank component, and N_i denotes the Gaussian noise matrix. Then we apply the proposed WSNM model to estimateX_i, and its corresponding optimization problem can be defined as:

$$\hat{X}_i = \arg\min_{X_i} \frac{1}{2}\left\| \hat{Y}_i - X_i \right\|_F^2 + \lambda_i \|X_i\|_{ws}^p, \tag{8}$$

where λ_i denotes the regularization parameter. The WSNM model can be solved by Eq. (7). Then, we define $\tau_i = \lambda_i w_i$. The parameter τ_i can be set empirically. However, a more reasonable and adaptive setting of this parameter could improve the recovery image quality. For better recovery performance, the parameter τ_i should be adaptively determined. According to previous subsection, Eq. (8) can be expressed as:

$$\hat{x}_i = \arg\min_{x_i} \sum_{j=1}^{m} \frac{1}{2}\left\| \hat{y}_{i,j} - U_i \delta_{i,j} v_{i,j}^T \right\|_2^2 + \tau_i |\delta_{i,j}|^p, \tag{9}$$

where $X_i = U_i \Delta_i V_i^T$ is the SVD of dataset X_i, $\Delta_i = \mathrm{diag}(\delta_{i,1}, \delta_{i,2}, \cdots \delta_{i,m})$ and $v_{i,j}$is the j-th of V_i. The regularization parameter can be derived by the Maximum a Posterior (MAP) estimator according to [32]. We extend the derivation to set an adaptive regularization parameter τ_i via Bayesian interpretation.

The MAP estimation of δ_i can be formulated as:

$$\delta_{\hat{Y}_i} = \arg\max_{\delta_i} \log P\left(\delta_i \middle| \hat{Y}_i \right) = \arg\max_{\delta_i} \left\{ \log P\left(\hat{Y}_i | \delta_i \right) + \log P(\delta_i) \right\}, \tag{10}$$

where δ_i is the concatenation of $\delta_{i,\ j}$. The likelihood term is characterized by the jointly Gaussian distribution:

$$P\left(\hat{Y}_i | \delta_i \right) = \prod_{j=1}^{m} \frac{1}{\sqrt{2\pi}\sigma_w} \exp\left(-\frac{1}{2\sigma_w^2} \left\| \hat{y}_{i,j} - U_i \delta_{i,j} v_{i,j}^T \right\|_2^2 \right), \tag{11}$$

where σ_w denotes the standard variance of the additive Gaussian noise. It can be empirically found that δ_i is nearly uncorrelated [12]. The prior term can be expressed by the Laplacian distribution:

$$P(\delta_i) = \prod_{j=1}^{m} \left\{ \frac{1}{\sqrt{2\pi}\sigma_i} \exp\left(-\frac{|\delta_{i,j}|}{\sigma_i} \right) \right\}, \tag{12}$$

where σ_i is the standard deviation of $\delta_{i,\ j}$.

Substituting Eqs. (11) and (12) into Eq. (10), we can obtain

$$\delta_{\hat{Y}_i} = \arg\min_{\delta_i} \sum_{j=1}^{m} \left(\left\| \hat{y}_{i,j} - U_i \delta_{i,j} v_{i,j}^T \right\|_2^2 + 2\sqrt{2}\sigma_w^2 \frac{1}{\sigma_i |\delta_{i,j}|^{p-1}} |\delta_{i,j}|^p \right). \tag{13}$$

Then, the sparsity of Rank(X_i) can be estimated by:

$$\hat{x}_i = \arg\min_{x_i} \sum_{j=1}^{m} \left(\left\| \hat{y}_{i,j} - U_i \delta_{i,j} v_{i,j}^T \right\|_2^2 + \frac{2\sqrt{2}\sigma_w^2}{\sigma_i^p} |\delta_{i,j}|^p \right). \tag{14}$$

Comparing Eqs. (9) and (14), we have

$$\tau_i = 2\sqrt{2}\sigma_w^2/\sigma_i^p. \tag{15}$$

4.2 Modeling of CS recovery

According to Eqs.(2) and (9), the objective function of CS recovery can be formulated as:

$$\left(\hat{x}, \hat{U}_i, \hat{\delta}_i, \hat{v}_{i,j}\right) = \arg\min_{x, U_i, \delta_i, v_{i,j}} \|y - \Phi x\|_2^2 + \beta \sum_i \sum_{j=1}^m \left(\frac{1}{2}\left\|R_{i,j}x - U_i \delta_{i,j} v_{i,j}^T\right\|_2^2 + \tau_i \left|\delta_{i,j}\right|^p\right), \tag{16}$$

where β is an adaptive regularization parameter and the measurement matrix Φ is a partial Fourier transform matrix. Eq. (16) can be solved via separating the image x and $\{\delta_i\}$. Then we apply the variable-splitting scheme to solve this optimization problem.

A. To solve the variable $\delta_{i,j}$, $v_{i,j}$ and U_i with fixing $x^{(k)}$, the optimization problem can be simplified to Eq.(8), and it can be solved via Eq.(7).

B. To solve the variable $x^{(k+1)}$ with fixing the other variables, the following quadratic optimization problem has a closed form solution:

$$\hat{x}^{(k+1)} = \arg\min_x \|y - \Phi x\|_2^2 + \beta \sum_i \sum_{j=1}^m \left(\left\|R_{i,j}x - \hat{U}_i \hat{\delta}_{i,j} \hat{v}_{i,j}^T\right\|_2^2\right), \tag{17}$$

$$\hat{x}^{(k+1)} = \frac{\Phi^T y + \beta \sum_i \sum_{j=1}^m R_{i,j}^T \hat{U}_i \hat{\delta}_{i,j} \hat{v}_{i,j}^T}{\Phi^T \Phi + \beta \sum_i \sum_{j=1}^m R_{i,j}^T R_{i,j}}. \tag{18}$$

These two steps iterate until convergence, and the algorithm is summarized in Algorithm 1.

Algorithm 1

Input : Observation y

Initialize $\hat{x}^{(0)}, \hat{y}^{(0)}$;

for $k = 1$: K do

  Iterative regularization $\hat{y}^{(k+1)} = \hat{x}^{(k)} + \delta^T \Phi^T (y - \Phi \hat{y}^{(k)})$;

  for each patch $\hat{y}_j^{(k+1)} \in \hat{y}^{(k+1)}$ do

    Find similar patch group $\hat{Y}_j$;

    Singular value decomposition $[\hat{U}_j^{(k+1)}, \hat{\Lambda}_j^{(k+1)}, \hat{V}_j^{(k+1)}] = SVD(\hat{Y}_j)$;

    Calculate $D_p^{GSVST}(\sigma_i^{k+1})$;

    Get the estimation: $\hat{X}_j^{(k+1)} = \hat{U}_j^{(k+1)} D_p^{GSVST}(\sigma_i^{k+1})(\hat{V}_j^{(k+1)})^T$.

  end

Aggregate $\hat{X}_j^{(k+1)}$ to form the reconstructed image $\hat{x}^{(k+1)}$ by Eq. (18);

end

Output: Reconstructed image $\hat{x}^{(K)}$.

5 Experimental results

This section presents extensive experimental validation of the proposed image compressed sensing method. The six test natural images and subsampling masks are shown in Fig. 1. The numerical results are presented for solving problem (16) with $0 < p \leq 1$. Moreover, to illustrate the advantages of the WSNM, we compare the results optimized using the proposed model with those using the standard nuclear norm. The proposed nonlocal low-rank regularization based CS method denoted as WSNM-CS. And let NNM-CS denote the nonlocal low-rank regularization using the standard nuclear norm. Finally, both qualitative and quantitative methods are used to evaluate the performance of the proposed method in comparison with several state-of-the-art CS methods. The CS measurements are generated by random subsampling and radial subsampling the Fourier transform coefficients of test images. The number of compressive measurements M is measured by the percentages of total number of image pixels N or Fourier coefficients.

Several parameters need to be set in the proposed algorithm. To reduce the computational complexity, we empirically set patch size to 6×6 and extract exemplar image patch in every 5 pixels along both horizontal and vertical directions. The number of similar patches is set to 45 for each exemplar patch.

5.1 Advantages of the weighted Schatten *p*-norm minimization

To illustrate the advantages of the proposed weighted Schatten p-norm minimization, we compare the proposed method WSNM-CS with NNM-CS for CS recovery. We choose $p = 0.9$, $M = 0.05\,N$ randomly for this experiment. Of course, it is necessary to analyze the influence of the changing power p upon the quality of CS recovery at different compressive measurements M. We test this in next experiments. In this experiment, we generate CS measurements by randomly sampling the Fourier transform coefficients of input natural images [5]. The peak signal-to-noise ratio (PSNR) results are shown in Table 1.

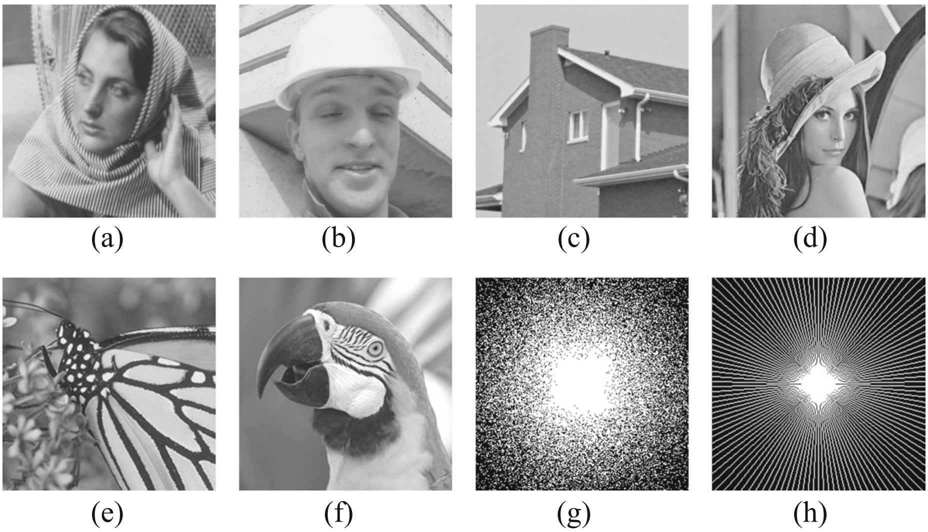

Fig. 1 Test images and subsampling masks. **a** Barbara. **b** Foreman. **c** House. **d** Lena. **e** Monarch. **f** Parrot **g** random subsampling mask. **h** radial subsampling mask

Table 1 The PSNR results of the WSNM-CS and NNM-CS methods

Method	Barbara	Foreman	House	Lena	Monarch	Parrots	Average
NNM-CS	27.68	35.08	33.31	28.84	26.99	30.42	30.39
WSNM-CS	29.49	35.34	34.10	30.17	28.61	31.85	31.59

From Table 1 we can see that, by using the WSNM surrogate of the rank, the proposed WSNM-CS method performs better than the NNM-CS method on all test images. On the average, the WSNM-CS can outperform the NNM-CS by up to 1.2 dB. Therefore, it is demonstrated that the NNM suppress the singular values and lead to the shrinkage of the recovery data, and the weighted Schatten p-norm relaxation is closer to the real solution of original rank minimization problem.

It is necessary for us to analyze the suitable setting of power p for each sensing rate. It can provide guidance for choosing optimal p for different compressive measurements. So, we randomly select 20 images, random subsampling, and test the proposed WSNM with different power p under different sensing rates. In each subfigure of Fig. 2, horizontal coordinate denotes the values of power p changing from 0.1 to 1 with interval 0.1, vertical coordinate represents the average PSNR. In this test, six sensing rates $M = \{0.05\,N, 0.1\,N, 0.15\,N, 0.2\,N, 0.25\,N, 0.3\,N\}$ are used. Then, take *Barbara* as an example, the reconstruction results in Fig. 3 show the influence of changing power p, as $M = 0.15\,N$.

As demonstrated in first five subfigures of Fig. 2, the optimal value for p is 0.8 when handling these low compressive measurements. Therefore we can conclude that the non-convex relaxation of the rank minimization is superior to the traditional tightest convex relaxation. For medium compressive measurements $M = 0.3\,N$, as the PSNR results shown in the last subfigure of Fig. 2, $p = 0.9$ is better. These empirical values are applied in the next subsection. Moreover, from Fig. 3, we can see that, texture can be recovered clearly when $p = 0.8$, and it produces less artifacts on the recovered image. To sum up, the value of power p is critical to the recovery quality, and has the relationship with the sensing rate.

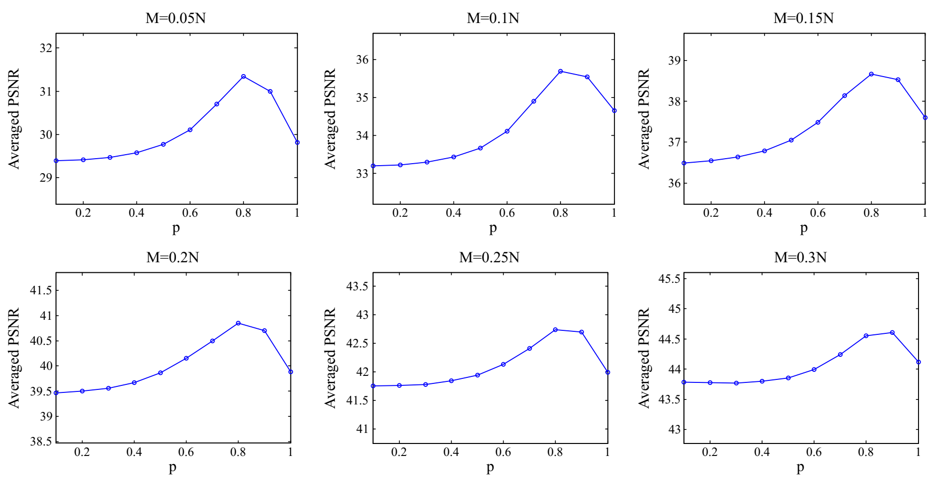

Fig. 2 The influence of changing p upon recovery results under different compressive measurements on 20 images

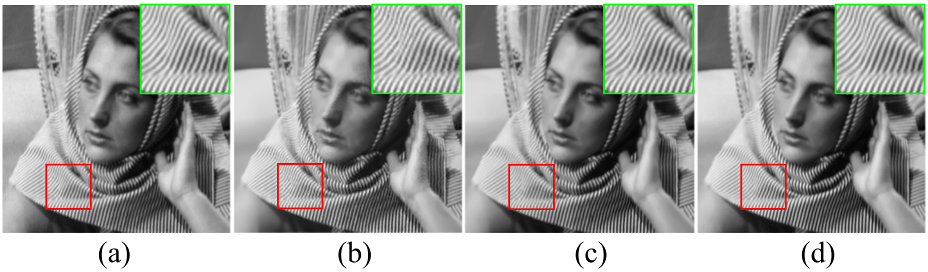

Fig. 3 CS recovered Barbara images with 0.15 N measurements (random sampling). **a** Original image. **b** Proposed WSNM-CS recovery (p = 0.2, 34.22 dB). **c** Proposed WSNM-CS recovery (p = 0.8, 38.22 dB) (dB). **d** Proposed WSNM-CS recovery (p = 1, 37.18 dB)

5.2 Comparison with conventional CS recovery methods

To verify the performance of the proposed nonlocal low-rank regularization based CS method, the proposed method is compared with some conventional CS recovery methods. These

Table 2 The PSNR (dB) results of test CS recovery methods with random subsampling scheme

Image	Method	Number of measurements					
		$M = 0.05\ N$	$M = 0.1\ N$	$M = 0.15\ N$	$M = 0.2\ N$	$M = 0.25\ N$	$M = 0.3\ N$
Barbara	TV	22.68	24.81	26.59	28.79	31.12	33.81
	ReTV	22.51	24.83	26.75	29.41	31.9	34.58
	MARX-PC	24.21	30.35	33.82	36.08	37.95	39.75
	BM3D-CS	24.45	29.02	33.11	36.12	38.55	40.59
	WSNM-CS	**29.85**	**35.42**	**38.22**	**40.08**	**41.61**	**43.12**
Foreman	TV	32.55	35.98	38.41	40.2	42.42	44.68
	ReTV	32.68	36.12	38.83	40.76	42.81	45.12
	MARX-PC	35.14	37.96	40.39	42.12	43.54	45.58
	BM3D-CS	33.12	36.62	39.11	40.45	42.08	44.21
	WSNM-CS	**36.08**	**39.49**	**42.06**	**44.11**	**46.12**	**48.42**
House	TV	30.35	33.58	35.32	37.28	38.89	40.86
	ReTV	30.87	33.76	35.59	37.35	39.11	41.09
	MARX-PC	32.79	35.29	36.89	38.73	40.46	42.47
	BM3D-CS	32.46	36.01	38.23	39.86	41.35	42.87
	WSNM-CS	**34.91**	**38.37**	**40.67**	**42.51**	**44.32**	**45.99**
Lena	TV	26.39	29.52	32.54	34.52	37.38	39.61
	ReTV	26.52	29.76	32.81	35.08	37.62	40.24
	MARX-PC	29.18	33.25	36.09	38.07	40.39	42.19
	BM3D-CS	27.18	31.54	35.62	38.13	40.23	42.44
	WSNM-CS	**30.93**	**35.77**	**39.01**	**41.45**	**43.49**	**45.35**
Monarch	TV	24.18	28.63	31.98	34.65	37.32	39.61
	ReTV	24.41	29.32	32.46	35.21	37.83	40.26
	MARX-PC	27.12	31.22	34.86	36.51	39.01	41.27
	BM3D-CS	24.62	29.53	34.05	37.16	39.52	41.79
	WSNM-CS	**28.65**	**34.14**	**37.79**	**40.32**	**42.45**	**44.21**
Parrot	TV	27.71	31.64	34.68	37.12	39.52	41.78
	ReTV	28.39	32.55	35.21	37.83	39.96	42.13
	MARX-PC	27.63	34.08	36.49	38.51	40.46	42.32
	BM3D-CS	29.11	33.59	36.49	38.92	40.91	42.65
	WSNM-CS	**32.52**	**36.67**	**39.61**	**41.45**	**43.25**	**44.79**
Average	TV	27.31	30.69	33.25	35.43	37.78	40.06
	ReTV	27.56	31.06	33.61	35.94	38.21	40.57
	MARX-PC	29.35	33.69	36.42	38.34	40.30	42.26
	BM3D-CS	28.49	32.72	36.10	38.44	40.44	42.43
	WSNM-CS	**32.16**	**36.64**	**39.56**	**41.65**	**43.54**	**45.31**

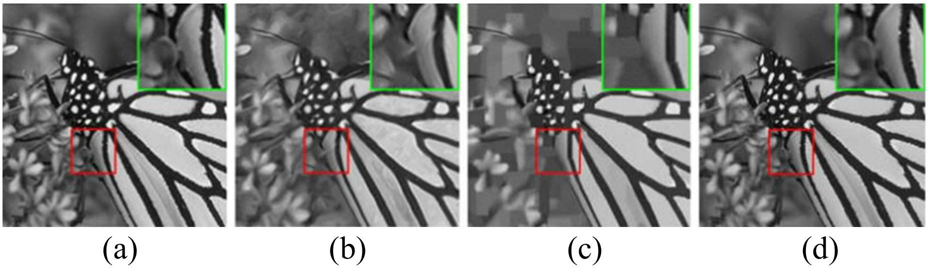

Fig. 4 CS recovered Monarch images with 0.1 N measurements (random sampling). **a** Original image. **b** MARX-PC recovery (31.22 dB). **c** BM3D-CS recovery (29.53 dB). **d** Proposed WSNM-CS recovery (34.14 dB)

methods include the total variation (TV) method, the iterative reweighted TV method, MARX-PC method and the BM3D based CS recovery method (denoted as BM3D-CS). The source codes of all benchmark methods [7, 16, 33, 38] were obtained from the authors' websites. To make a fair comparison among the competing methods, we have carefully tuned their parameters to achieve the best performance. For WSNM-CS, according to the analysis of the power p (discussed in Section 5.1), we choose $p = \{0.8,0.9\}$ for $M \leq 0.25\ N$ and $0.3\ N \leq M$, respectively. The PSNR results of competing CS recovery methods with random subsampling scheme are reported in Table 2 (The highest PSNR values are marked in bold to facilitate the comparison). To facilitate the evaluation of subjective qualities, partial reconstructed images are shown in Figs. 4 and 5.

It can be observed from Table 2 that ReTV outperforms conventional TV on almost all test images. BM3D-CS and MARX-PC methods generally perform better. The proposed WSNM-CS method, using the weighted Schatten p-norm minimization, achieves the highest PSNR in all test images and sensing rates. It is also observed that the PSNR gains of WSNM-CS outperform the BM3D-CS and MARX-PC by 2.14 dB ~ 6.4 dB and 0.94 dB ~5.64 dB respectively. And the most favorable situation is on the *Barbara* image. Moreover, when using less CS measurements, the proposed WSNM-CS can produce higher PSNRs than other competing methods. As shown in Fig. 4c, the conventional BM3D-CS leads to obvious artifacts, and the proposed method does not introduce obvious aliasing artifacts. Moreover, it preserves the fine edges and small-scale fine structures as shown in Figs. 4d and 5d. In summary, the proposed WSNM-CS method outperforms other methods in term of better image quality and lower reconstruction errors. These results also show that the proposed WSNM can remedy the suppression problem of the NNM to some extent.

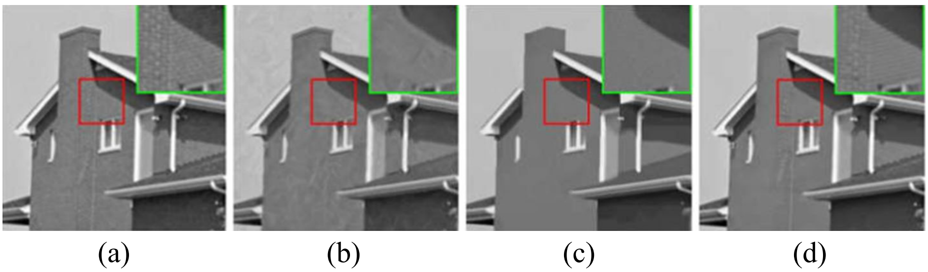

Fig. 5 CS recovered House images with 0.1 N measurements (random sampling). **a** Original image. **b** MARX-PC recovery (35.29 dB). **c** BM3D-CSrecovery (36.01 dB). **d** Proposed WSNM-CS recovery (38.37 dB)

Table 3 The PSNR (dB) results of test CS recovery methods with radial subsampling scheme

Image	Method	Number of measurements					
		$M = 0.08\ N$ 20 lines	$M = 0.13\ N$ 35 lines	$M = 0.14\ N$ 50 lines	$M = 0.24\ N$ 65 lines	$M = 0.29\ N$ 80 lines	$M = 0.34\ N$ 95 lines
Barbara	TV	21.73	23.04	23.82	24.42	25.38	26.55
	ReTV	21.35	22.85	23.68	24.12	25.1	26.48
	MARX-PC	21.04	22.92	24.13	25.53	29.08	32.49
	BM3D-CS	21.78	24.41	28.34	31.12	33.57	34.9
	WSNM-CS	**23.79**	**27.24**	**29.16**	**29.98**	**31.33**	**32.51**
Foreman	TV	28.82	32.45	35.39	37.14	38.62	39.95
	ReTV	29.31	33.11	35.67	37.47	38.91	40.09
	MARX-PC	29.59	34.13	37.28	38.39	39.98	41.17
	BM3D-CS	29.83	34.67	37.31	38.9	40.08	40.69
	WSNM-CS	**31.88**	**36.09**	**38.99**	**40.4**	**41.67**	**43.05**
House	TV	28.16	30.76	33.24	34.75	35.39	36.81
	ReTV	28.75	31.18	33.46	34.83	35.41	36.74
	MARX-PC	29.31	32.04	34.74	35.98	36.69	37.91
	BM3D-CS	30.84	32.71	35.86	36.55	37.24	38.16
	WSNM-CS	**32.11**	**34.2**	**36.06**	**37.58**	**37.92**	**39.37**
Lena	TV	23.15	26.14	28.97	30.59	32.32	33.72
	ReTV	23.29	26.32	29.26	30.87	32.56	33.83
	MARX-PC	23.73	27.38	31.21	32.83	35.17	36.44
	BM3D-CS	23.31	27.42	30.96	33.08	35.19	36.39
	WSNM-CS	**25.15**	**29.6**	**33.07**	**35.52**	**37.83**	**39.03**
Monarch	TV	18.85	24.29	28.23	30.59	32.96	34.41
	ReTV	19.07	24.79	28.63	31.11	33.37	34.7
	MARX-PC	19.64	25.85	29.91	31.85	33.96	35.31
	BM3D-CS	19.67	26.36	30.46	32.76	35.21	35.97
	WSNM-CS	**20.14**	**28.28**	**32.69**	**35.51**	**37.71**	**39.06**
Parrot	TV	24.29	28.53	31.64	33.58	35.41	36.52
	ReTV	24.35	28.97	32.15	33.86	35.61	36.85
	MARX-PC	24.96	30.86	33.45	35.07	36.43	37.63
	BM3D-CS	25.25	30.21	34.28	36.01	37.44	38.42
	WSNM-CS	**27.96**	**32.91**	**35.76**	**37.52**	**38.91**	**40.13**
Average	TV	24.17	27.54	30.22	31.85	33.35	34.66
	ReTV	24.35	27.87	30.48	32.04	33.49	34.78
	MARX-PC	24.71	28.86	31.79	33.28	35.22	36.83
	BM3D-CS	25.11	29.30	32.87	34.74	36.46	37.42
	WSNM-CS	**26.84**	**31.39**	**34.29**	**36.09**	**37.56**	**38.86**

Then, the CS measurements are generated by radial subsampling. The PSNR results of reconstructed images under radial subsampling scheme are shown in Table 3.

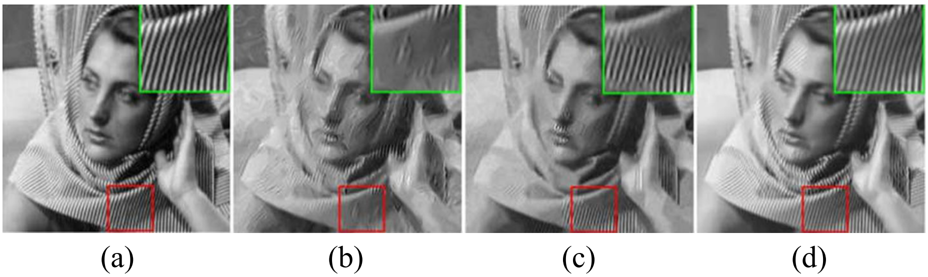

Fig. 6 CS recovered Barbara images with radial subsampling (35 radial lines, i.e., 0.13 N measurements). **a** Original image. **b** MARX-PC recovery (22.92 dB). **c** BM3D-CSrecovery (24.41 dB). **d** Proposed WSNM-CS recovery (27.24 dB)

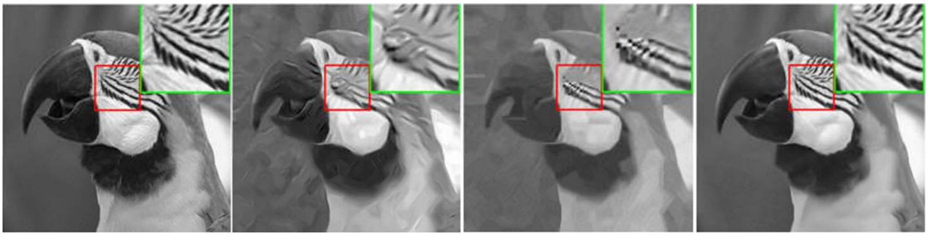

Fig. 7 CS recovered Parrots images with radial subsampling (35 radial lines, i.e., 0.13 N measurements). **a** Original image. **b** MARX-PC recovery (30.86 dB). **c** BM3D-CS recovery (30.21 dB). **d** Proposed WSNM-CS recovery (32.91 dB)

As can be seen from Tables 2 and 3, the average PSNR gains of the proposed method with random subsampling and radial subsampling are 39.87 dB and 34.17 dB respectively. These results show that radial subsampling produces streaking artifacts, which are more difficult to remove. However, from Table 3, it is easy to observe that the proposed method produces the highest PSNRs on all test images and CS measurement rates. The average PSNR improvements over BM3D-CS and MARX-PC are about 1.52 dB and 2.39 dB, respectively. Partial reconstructed images on the radial subsampling case are shown in Figs. 6 and 7. These results indicate that MARX-PC and BM3D-CS cannot reduce streaking artifacts efficiently. The WSNM-CS reconstructed images obtain clear edge structures. It is worth mentioning that reconstructed result in Fig. 7d has better fine features and more clear directions than that in Fig. 7b, c.

NLR-CS [14] also applied nonlocal low-rank regularization for CS, and log det($\boldsymbol{X}$) was used as a surrogate function for the rank. However, WSNM is used for non-convex low-rank approximation in the proposed method. Thus, the CS recovery model and optimization algorithm of the WSNM-CS are different with the NLR-CS. Then these two methods are compared through PSNR, structural similarity (SSIM) index and computation time in seconds. The comparison results are shown in Tables 4, 5 and 6. From Table 4, we can see that the proposed WSNM-CS achieves the higher PSNR in almost cases. When the numbers of

Table 4 The PSNR (dB) results of test CS recovery methods with random subsampling scheme

Image	Method	Number of measurements					
		0.05 N	0.1 N	0.15 N	0.2 N	0.25 N	0.3 N
Barbara	NLR-CS	29.81	**35.47**	38.19	40.04	41.54	43.06
	WSNM-CS	**29.85**	35.42	**38.22**	**40.08**	**41.61**	**43.12**
Foreman	NLR-CS	35.83	39.42	41.99	44.03	**46.13**	**48.45**
	WSNM-CS	**36.08**	**39.49**	**42.06**	**44.11**	46.12	48.42
House	NLR-CS	34.81	**38.39**	40.65	42.49	44.31	45.95
	WSNM-CS	**34.91**	38.37	**40.67**	**42.51**	**44.32**	**45.99**
Lena	NLR-CS	30.72	35.75	38.98	41.40	43.48	**45.38**
	WSNM-CS	**30.93**	**35.77**	**39.01**	**41.45**	**43.49**	45.35
Monarch	NLR-CS	**28.84**	**34.30**	**37.86**	40.32	42.41	44.17
	WSNM-CS	28.65	34.14	37.79	**40.32**	**42.45**	**44.21**
Parrots	NLR-CS	32.46	36.62	39.58	41.44	43.23	44.76
	WSNM-CS	**32.52**	**36.67**	**39.61**	**41.45**	**43.25**	**44.79**
Average	NLR-CS	32.08	36.66	39.54	41.62	43.52	45.30
	WSNM-CS	**32.16**	**36.64**	**39.56**	**41.65**	**43.54**	**45.31**

Table 5 The SSIM results of test CS recovery methods with random subsampling scheme

Image	Method	Number of measurements					
		0.05 N	0.1 N	0.15 N	0.2 N	0.25 N	0.3 N
Barbara	NLR-CS	0.87902	**0.95803**	0.97367	0.98066	0.98491	0.98846
	WSNM-CS	**0.87915**	0.95758	**0.97395**	**0.98081**	**0.98520**	**0.98912**
Foreman	NLR-CS	0.92036	0.95403	0.97176	0.98134	0.98800	**0.99269**
	WSNM-CS	**0.92352**	**0.95483**	**0.97236**	**0.98178**	**0.98805**	0.99264
House	NLR-CS	0.87711	**0.93939**	0.96209	0.97451	0.98275	0.98765
	WSNM-CS	**0.87857**	0.93857	**0.96258**	**0.97461**	**0.98282**	**0.98790**
Lena	NLR-CS	0.87932	0.94632	0.96935	0.97890	0.98602	**0.99023**
	WSNM-CS	**0.88328**	**0.94682**	**0.96950**	**0.98014**	**0.98613**	0.99017
Monarch	NLR-CS	**0.89319**	**0.95669**	**0.97405**	0.98164	0.98663	0.98995
	WSNM-CS	0.89260	0.95645	0.97397	**0.98165**	**0.98692**	**0.99056**
Parrots	NLR-CS	0.89238	0.94262	0.96425	0.97378	0.98079	0.98527
	WSNM-CS	**0.89553**	**0.94369**	**0.96490**	**0.97416**	**0.98095**	**0.98559**
Average	NLR-CS	0.89023	0.94951	0.96920	0.97847	0.98485	0.98904
	WSNM-CS	**0.89211**	**0.94966**	**0.96954**	**0.97886**	**0.98501**	**0.98933**

measurement is 0.05 N, the improvement of WSNM-CS over NLR-CS is 0.08 dB on average, respectively. The SSIM is based on the idea that a measure of change in structural information is a good approximation to perceived quality change. As can be seen from Table 5, the results of these two methods are similar. The SSIM of NLR-CS and WSNM-CS can reach 0.99269 and 0.99264, respectively. The programs run on 10 Cores 2.6GHz CPU workstation with 64GB RAM. In term of the computation time, the WSNM-CS is longer than NLR-CS, for calculating$D_p^{GSVST}\left(\sigma_i^{k+1}\right)$takes some time. These two methods were not optimized, and the main computational cost of them is the computation of the singular value decomposition. The corresponding comparison results with radial subsampling are not present in the following paragraph, because they are similar with the results with random subsampling scheme.

6 Conclusion

In this paper, a weighted Schatten p-norm minimization based low-rank approximation method has been proposed for CS recovery. Both the nonlocal sparsity of similar patches and the non-convexity of weighted Schatten p-norm are utilized via nonlocal low-rank regularization. Moreover, the weighted Schatten p-norm, as a non-convex relaxation, improves the low rank property of matrix, which is equivalent to the sparsity of singular values. Experimental results demonstrate that the proposed method can achieve highly competitive performance to the recently CS recovery methods.

Table 6 The average computation time results of test CS recovery methods with random subsampling scheme

Image	Method	Number of measurements					
		0.05 N	0.1 N	0.15 N	0.2 N	0.25 N	0.3 N
Average	NLR-CS	251.2517	260.9583	224.8567	185.6367	148.6867	142.7767
	WSNM-CS	432.185	343.7033	276.7483	202.5233	166.915	153.8183

Acknowledgements The authors would like to give thanks to the anonymous reviewers for their valuable comments that were useful to improve the quality of the paper. This work was supported by Natural Science Foundation of Tianjin (Grant No. 15JCYBJC15500).

References

1. Baraniuk RG, Cevher V, Duarte MF, Hegde C (2010) Model-based compressive sensing. IEEE Trans Inf Theory 56(4):1982–2001
2. Buades A, Coll B, Morel JM (2005) A review of image denoising algorithms, with a new one. Multiscale Modeling & Simulation 4(2):490–530
3. Cai JF, Candès EJ, Shen Z (2010) A singular value thresholding algorithm for matrix completion. SIAM J Optim 20(4):1956–1982
4. Candès EJ, Recht B (2009) Exact matrix completion via convex optimization. Found Comput Math 9(6): 717–772
5. Candès EJ, Romberg J (2005) Practical signal recovery from random projections. Proc SPIE Comput Imag 5674:76–86
6. Candès EJ, Romberg J, Tao T (2006) Robust uncertainty principles: exact signal reconstruction from highly incomplete frequency information. IEEE Trans Inf Theory 52(2):489–509
7. Candès EJ, Wakin MB, Boyd SP (2008) Enhancing sparsity by reweighted ℓ1 minimization. J Fourier Anal Appl 14(5–6):877–905
8. Candès EJ, Li X, Ma Y, Wright J (2011) Robust principal component analysis? J ACM 58(3):11
9. Chen SS, Donoho DL, Saunders MA (2001) Atomic decomposition by basis pursuit. SIAM Rev 43(1):129–159
10. Dabov K, Foi A, Katkovnik V, Egiazarian K (2007) Image denoising by sparse 3-D transform-domain collaborative filtering. IEEE Trans Image Process 16(8):2080–2095
11. Daubechies I, Defrise M, De Mol C (2004) An iterative thresholding algorithm for linear inverse problems with a sparsity constraint. Commun Pure Appl Math 57(11):1413–1457
12. Dong W, Zhang L, Shi G (2011) Centralized sparse representation for image restoration. In 2011 International Conference on Computer Vision, pp 1259–1266
13. Dong W, Shi G, Li X, Zhang L, Wu X (2012) Image reconstruction with locally adaptive sparsity and nonlocal robust regularization. Signal Process Image Commun 27(10):1109–1122
14. Dong W, Shi G, Li X, Ma Y, Huang F (2014) Compressive sensing via nonlocal low-rank regularization. IEEE Trans Image Process 23(8):3618–3632
15. Donoho DL (2006) Compressed sensing. IEEE Trans Inf Theory 52(4):1289–1306
16. Egiazarian K, Foi A, Katkovnik V (2007) Compressed sensing image reconstruction via recursive spatially adaptive filtering. In 2007 I.E. International Conference on Image Processing, 1, pp I-549–I-552
17. Foucart S, Lai MJ (2009) Sparsest solutions of underdetermined linear systems via ℓq-minimization for 0<q⩽1. Appl Comput Harmon Anal 26(3):395–407
18. Gu S, Zhang L, Zuo W, Feng X (2014) Weighted nuclear norm minimization with application to image denoising. In 2014 I.E. Conference on Computer Vision and Pattern Recognition, pp 2862–2869
19. Huang J, Zhang T, Metaxas D (2011) Learning with structured sparsity. J Mach Learn Res 12:3371–3412
20. Jiang J, Ma X, Chen C, Lu T, Wang Z, Ma J (2017) Single image super-resolution via locally regularized anchored neighborhood regression and nonlocal means. IEEE Trans Multimedia 19(1):15–26
21. Lin Z, Chen M, Wu L, Ma Y (2009) The augmented Lagrange multiplier method for exact recovery of corrupted low-rank matrices. Dept. Electr. Comput. Eng., Univ. Illinois Urbana-Champaign, Urbana, IL, USA, Tech. Rep. UILU-ENG-09-2215
22. Liu R, Lin Z, De la Torre F, Su Z (2012, June) Fixed-rank representation for unsupervised visual learning. In 2012 I.E. Conference on Computer Vision and Pattern Recognition, pp 598–605
23. Liu L, Huang W, Chen DR (2014) Exact minimum rank approximation via Schatten p-norm minimization. J Comput Appl Math 267:218–227
24. Lu YM, Do MN (2008) Sampling signals from a union of subspaces. IEEE Signal Process Mag 25(2):41–47
25. Lu T, Xiong Z, Wan Y, Yang W (2016) Face hallucination via locality-constrained low-rank representation. In 2016 I.E. international conference on acoustics, speech and signal processing, pp. 1746-1750
26. Mairal J, Bach F, Ponce J, Sapiro G, Zisserman A (2009) Non-local sparse models for image restoration. In 2009 I.E. 12th International Conference on Computer Vision, pp 2272–2279
27. Massa A, Rocca P, Oliveri G (2015) Compressive sensing in electromagnetics-a review. IEEE Antennas and Propagation Magazine 57(1):224–238
28. Mirsky L (1975) A trace inequality of John von Neumann. Monatshefte für Mathematik 79(4):303–306

29. Natarajan BK (1995) Sparse approximate solutions to linear systems. SIAM J Comput 24(2):227–234
30. Nie F, Wang H, Cai X, Huang H, Ding C (2012, December) Robust matrix completion via joint schatten p-norm and lp-norm minimization. In 2012 I.E. 12th International Conference on Data Mining, pp 566–574
31. Pan JS, Li W, Yang CS, Yan LJ (2015) Image steganography based on subsampling and compressive sensing. Multimedia Tools and Applications 74(21):9191–9205
32. Sendur L, Selesnick IW (2002) Bivariate shrinkage functions for wavelet-based denoising exploiting interscale dependency. IEEE Trans Signal Process 50(11):2744–2756
33. Software l1magic [Online] (2006) Available: http://www.acm.caltech.edu/l1magic
34. Tropp J, Gilbert AC (2005) Signal recovery from partial information via orthogonal matching pursuit
35. Wang Y, Wang J, Xu Z (2014) Restricted p-isometry properties of nonconvex block-sparse compressed sensing. Signal Process 104:188–196
36. Wang B, Lu T, Xiong Z (2016) Adaptive boosting for image denoising: Beyond low-rank representation and sparse coding. In 2016 International Conference on Pattern Recognition
37. Wipf DP, Rao BD (2004) Sparse Bayesian learning for basis selection. IEEE Trans Signal Process 52(8):2153–2164
38. Wu X, Dong W, Zhang X, Shi G (2012) Model-assisted adaptive recovery of compressed sensing with imaging applications. IEEE Trans Image Process 21(2):451–458
39. Xie Y, Gu S, Liu Y, Zuo W, Zhang W, Zhang L (2015) Weighted Schatten p-norm minimization for image Denoising and background subtraction. arXiv preprint arXiv:1512.01003
40. Xu BH, Cen YG, Wei Z, Cen Y, Zhao RZ, Miao ZJ (2016) Video restoration based on PatchMatch and reweighted low-rank matrix recovery. Multimedia Tools and Applications 75(5):2681–2696
41. Zhang D, Hu Y, Ye J, Li X, He X (2012) Matrix completion by truncated nuclear norm regularization. In 2012 I.E. Conference on Computer Vision and Pattern Recognition, pp 2192–2199
42. Zhang J, Xiang Q, Yin Y, Chen C, Luo X (2016) Adaptive compressed sensing for wireless image sensor networks. Multimedia Tools and Applications: 1–16
43. Zuo W, Meng D, Zhang L, Feng X, Zhang D (2013) A generalized iterated shrinkage algorithm for non-convex sparse coding. In Proceedings of the IEEE international conference on computer vision, pp 217–224

Yan Zhang received the M.S. degree in circuit and system from the school of electronic information engineering, Tianjin University, Tianjin, China, in 2007. She is a lecturer in Tianjin Chengjian University, China. Currently, she is pursuing her Ph. D. degree from school of electronic information engineering, Tianjin University, China. Her research interests include compressive sensing and image processing.

Jichang Guo received the M.S. and Ph.D. degrees in signal and information processing from the school of electronic information engineering, Tianjin University, Tianjin, China, in 1993 and 2006, respectively. He is currently a full professor in Tianjin University. His current research interests include digital image processing, video coding, computer vision and compressive sensing.

Chongyi Li is pursuing his PhD degree in the school of Electronic Information Engineering, Tianjin University, Tianjin, China. His current research focuses on digital image processing, computer vision, and especially on underwater image enhancement and restoration.